



# A Trade-Off for Maintenance of Multidrug-Resistant IncHI2 Plasmids in *Salmonella enterica* Serovar Typhimurium through Adaptive Evolution

Jin-Fei Zhang,<sup>a,b</sup>  Liang-Xing Fang,<sup>a,b,c</sup> Man-Xia Chang,<sup>a,b</sup> Ming Cheng,<sup>a,b</sup> Hui Zhang,<sup>a,b</sup> Teng-Fei Long,<sup>a,b</sup> Qian Li,<sup>a,b</sup> Xin-lei Lian,<sup>a,b,c</sup>  Jian Sun,<sup>a,b,c</sup>  Xiao-Ping Liao,<sup>a,b,c</sup>  Ya-Hong Liu<sup>a,b,c,d</sup>

<sup>a</sup>National Risk Assessment Laboratory for Antimicrobial Resistance of Animal Original Bacteria, College of Veterinary Medicine, South China Agricultural University, Guangzhou, China

<sup>b</sup>Guangdong Provincial Key Laboratory of Veterinary Pharmaceutics Development and Safety Evaluation, South China Agricultural University, Guangzhou, China

<sup>c</sup>Guangdong Laboratory for Lingnan Modern Agriculture, Guangzhou, Guangdong, China

<sup>d</sup>Jiangsu Co-Innovation Center for the Prevention and Control of Important Animal Infectious Diseases and Zoonoses, Yangzhou University, Yangzhou, China

Jin-Fei Zhang and Liang-Xing Fang contributed equally to this work. Author order was determined by votes of all the authors.

**ABSTRACT** Understanding the fitness costs associated with plasmid carriage is a key to better understanding the mechanisms of plasmid maintenance in bacteria. In the current work, we performed multiple serial passages (63 days, 627.8 generations) to identify the compensatory mechanisms that *Salmonella enterica* serovar Typhimurium ATCC 14028 utilized to maintain the multidrug-resistant (MDR) IncHI2 plasmid pJXP9 in the presence and absence of antibiotic selection. The plasmid pJXP9 was maintained for hundreds of generations even without drug exposure. Endpoint evolved (the endpoint of evolution) *S. Typhimurium* bearing evolved plasmids displayed decreased growth lag times and a competitive advantage over ancestral pJXP9 plasmid-carrying ATCC 14028 strains. Genomic and transcriptomic analyses revealed that the fitness costs of carrying pJXP9 were derived from both specific plasmid genes and particularly the MDR regions and conjugation transfer region I and conflicts resulting from chromosome-plasmid gene interactions. Correspondingly, plasmid deletions of these regions could compensate for the fitness cost that was due to the plasmid carriage. The deletion extent and range of large fragments on the evolved plasmids, as well as the trajectory of deletion mutation, were related to the antibiotic treatment conditions. Furthermore, it is also adaptive evolution that chromosomal gene mutations and altered mRNA expression correlated with changed physiological functions of the bacterium, such as decreased flagellar motility, increased oxidative stress, and fumaric acid synthesis but increased Cu resistance in a given niche. Our findings indicated that plasmid maintenance evolves via a plasmid-bacterium adaptative evolutionary process that is a trade-off between vertical and horizontal transmission costs along with associated alterations in host bacterial physiology.

**IMPORTANCE** The current idea that compensatory evolution processes can account for the “plasmid paradox” phenomenon associated with the maintenance of large costly plasmids in host bacteria has attracted much attention. Although many compensatory mutations have been discovered through various plasmid-host bacterial evolution experiments, the basis of the compensatory mechanisms and the nature of the bacteria themselves to address the fitness costs remain unclear. In addition, the genetic backgrounds of plasmids and strains involved in previous research were limited and clinical drug resistance such as the poorly understood compensatory evolution among clinically dominant multidrug-resistant plasmids or clones was rarely considered. The IncHI2 plasmid is widely distributed in *Salmonella* Typhimurium and plays an important role in the emergence and rapid spread of its multidrug resistance. In this study, the predominant multidrug-resistant IncHI2 plasmid pJXP9 and

**Editor** Alejandra Rodríguez-Verdugo, University of California, Irvine

**Copyright** © 2022 Zhang et al. This is an open-access article distributed under the terms of the [Creative Commons Attribution 4.0 International license](https://creativecommons.org/licenses/by/4.0/).

Address correspondence to Ya-Hong Liu, lyh@scau.edu.cn, Xiao-Ping Liao, xpliao@scau.edu.cn, or Jian Sun, jiansun@scau.edu.cn.

The authors declare no conflict of interest.

**Received** 10 March 2022

**Accepted** 8 August 2022

**Published** 30 August 2022

the standard *Salmonella* Typhimurium ATCC 14028 bacteria were used for evolution experiments under laboratory conditions. Our findings indicated that plasmid maintenance through experimental evolution of plasmid-host bacteria is a trade-off between increasing plasmid vertical transmission and impairing its horizontal transmission and bacterial physiological phenotypes, in which compensatory mutations and altered chromosomal expression profiles collectively contribute to alleviating plasmid-borne fitness cost. These results provided potential insights into understanding the relationship of coexistence between plasmids encoding antibiotic resistance and their bacterial hosts and provided a clue to the adaptive forces that shaped the evolution of these plasmids within bacteria and to predicting the evolution trajectory of antibiotic resistance.

**KEYWORDS** IncHI2 plasmid, *Salmonella*, fitness cost, adaptive evolution, plasmid stability, compensatory mutation

Antibiotics have been a major accomplishment of modern medicine, but these compounds have suffered a loss of efficacy due to the emergence and dissemination of resistance among bacterial pathogens (1, 2). Therefore, novel strategies are needed to ensure clinical efficacy and to effectively curb the development and spread of bacterial resistance. Bacterial plasmids encode a wide range of phenotypic traits that allow bacteria to adapt to stressors such as the presence of antibiotics and have a key role in bacterial ecology and evolution (3). Interestingly, plasmids are maintained in bacterial populations over the long term, even in the absence of selection for plasmid-encoded traits. This “plasmid paradox” remains poorly understood, since plasmid carriage itself incurs physiological fitness costs to the host bacterium (4). Therefore, understanding the adaptive forces that shape the evolution of these plasmids within a bacterial host may explain the widespread distribution and stable maintenance of plasmids. This information could be used to predict the evolutionary trajectory of antibiotic resistance (5).

*Salmonella* is an important zoonotic pathogen, and currently, multidrug-resistant (MDR) strains that are resistant to fluoroquinolones, third-generation cephalosporins, and even colistin, such as *Salmonella enterica* serovar Typhimurium and its variants, have emerged (6, 7). Incompatibility HI2 (IncHI2) plasmids are often large (>200 kb) with similar backbone structures and possess two sets of conjugation systems along with numerous antibiotic resistance genes (ARGs) (8, 9). These IncHI2 plasmids are widespread among MDR *Enterobacteriaceae* and especially *S. Typhimurium*, even though they incur a high fitness cost for their maintenance (8–10).

In this study, we performed 63 serial passages to explore the compensatory mechanisms of adaptive evolution of the MDR IncHI2 plasmid pJXP9 within *S. Typhimurium* ATCC 14028 in the presence and absence of antibiotics. Our findings suggest that plasmid maintenance through plasmid-host bacterial coadaptation and coevolution is a trade-off but that coevolution of this large IncHI2 plasmid promoted host cell growth and competitiveness. This coevolution thereby increased plasmid vertical transmission by increasing host competitiveness and decreased growth lag times but impaired horizontal transmission of the plasmid and altered host bacterial physiology in a given niche. These results provide insights into understanding the mechanisms that bacteria use to offset the costs of stable plasmid maintenance.

## RESULTS

**Reducing lag time and improving competition advantage in evolved bacteria through plasmid-bacterium coadaptation.** The experimental system we used for this study was a comparison of the cost of maintaining a large IncHI2 plasmid (pJXP9) in *S. Typhimurium* strain ATCC 14028 with that of its plasmid-free counterpart. Preliminary experiments indicated that carriage of pJXP9 impaired competition and generated a slight growth disadvantage for strain ATCC 14028 (see Fig. S1 in the supplemental material). We extended these experiments and performed serial dilutions of cultures over

63 days in the presence and absence of antibiotics to investigate the stability of the IncHI2 plasmid in endpoint evolved clones/populations (clones/populations from the endpoint of evolution). Using PCR for 240 endpoint evolved clones and quantitative real-time PCR (qPCR) for 12 endpoint evolved populations, we found that IncHI2 plasmid pJXP9 was retained at day 63 with almost no loss when cultured in the presence of ciprofloxacin (CIP) and cefotaxime (CTX) but that plasmid levels were slightly reduced in the presence of colistin (CST) (24% loss using PCR and 7.7% loss using qPCR screening). Interestingly, culture in the absence of antibiotics led to significant plasmid loss (41.7% loss using PCR and 52.3% loss using qPCR screening) (Fig. 1A and B; Fig. S2). These results indicate that carriage of pJXP9 imposed a fitness cost, but the plasmid was maintained for at least hundreds of generations even in the absence of positive selection. To determine the fitness response to plasmid-bacterial host coevolution with or without antibiotic treatment, we directly competed 5 randomly selected endpoint evolved clones from each treatment (total, 20) against strain ATCC 14028::*lux*+pJXP9, which possessed a luciferase fluorescent marker integrated into the host chromosome. We found an increase in the competitive fitness in all 20 endpoint evolved clones (relative fitness [RF] range, 1.015 to 1.206) except one (RF = 0.7482) (Fig. 1C). These results revealed that adaptive evolution had occurred between the IncHI2 plasmid pJXP9 and the host, ATCC 14028.

To establish whether the fitness alterations were due to evolution of the plasmid, the bacterial host, or both, the evolved pJXP9 plasmids from evolved hosts were transferred to host ATCC 14028::*lux*, and 7 transconjugants carrying evolved plasmids were successfully obtained. The competitive fitness measurements for all these transconjugants remained less than those of ATCC 14028+pJXP9 (RF range, 0.88 to 1.01) (Fig. 1D). We further quantified the fitness levels for the 7 evolved clones and corresponding transconjugants using growth curves. Compared to the 7 transconjugants, the corresponding evolved clones displayed significant reductions in growth lag times (47.05 versus 54.30 min) ( $P < 0.05$ ) (Fig. 1E) but also a decreased growth rate (0.01059 versus 0.01076 per min) ( $P > 0.05$ ) (Fig. 1F) and a decreased maximum optical density at 600 nm (max OD<sub>600</sub>) (0.5109 versus 0.5594) ( $P < 0.05$ ) (Fig. 1G). In contrast, compared to the ancestral host ATCC 14028+pJXP9, the corresponding transconjugants of these evolved plasmids possessed higher growth rates (0.01131 versus 0.01076 per min) ( $P > 0.05$ ) (Fig. 1F) and max OD<sub>600</sub> values (0.5833 versus 0.5594) ( $P > 0.05$ ) (Fig. 1G) and decreased lag times (53.23 versus 54.30 min) ( $P > 0.05$ ) (Fig. 1E). Taken together, these findings suggest that evolution of both the plasmid and the host contribute to fitness effect changes in endpoint evolved clones. The competitive advantage and reduced lag times were primarily due to the evolved host, while carriage of the evolved pJXP9 plasmid slightly improved the growth rate and maximum culture density but impaired the competitive fitness.

**Diversity in large fragment deletions among plasmid MDR and conjugative transfer regions on evolved isolates.** To determine the contribution of pJXP9 plasmid evolution to cost alleviation, whole-genome sequencing (WGS) data of the pJXP9 plasmids from 20 endpoint evolved clones using 4 different antibiotic conditions were utilized to identify any gene deletions or additions that may have occurred during endpoint evolution experiments (Fig. 2A; Fig. S3). In general, the derived plasmids ranged in size from ~80 to ~244 kb, and the GC content tended to decline (see figure at <https://doi.org/10.6084/m9.figshare.20416359>). We identified six types of deletions and rearrangements. Type I included 3 clones with deletions of <30-kb fragments. The other five deletion types included the following plasmid regions: MDR region I (MDR I) ( $n = 3$ , type II), MDR region ( $n = 7$ , type III), MDR I and MDR region II (MDR II) and conjugative transfer region I ( $n = 4$ , type IV), MDR I and II and conjugative transfer region I ( $n = 1$ , type V), and an ~165-kb region including *repH12* ( $n = 2$ , type VI), which was found in two evolved clones, E-CST-572 and E-CST-574. Interestingly, deletion sizes were related to antibiotic selection as follows: CST, range of ~20 to ~165 kb; CTX, ~20 to ~50 kb; CIP, ~30 to ~90 kb; and no antibiotic, ~30 to ~79 kb (Fig. 2B). These results indicated a diversity of large fragment deletions for the plasmid MDR and conjugative transfer regions.

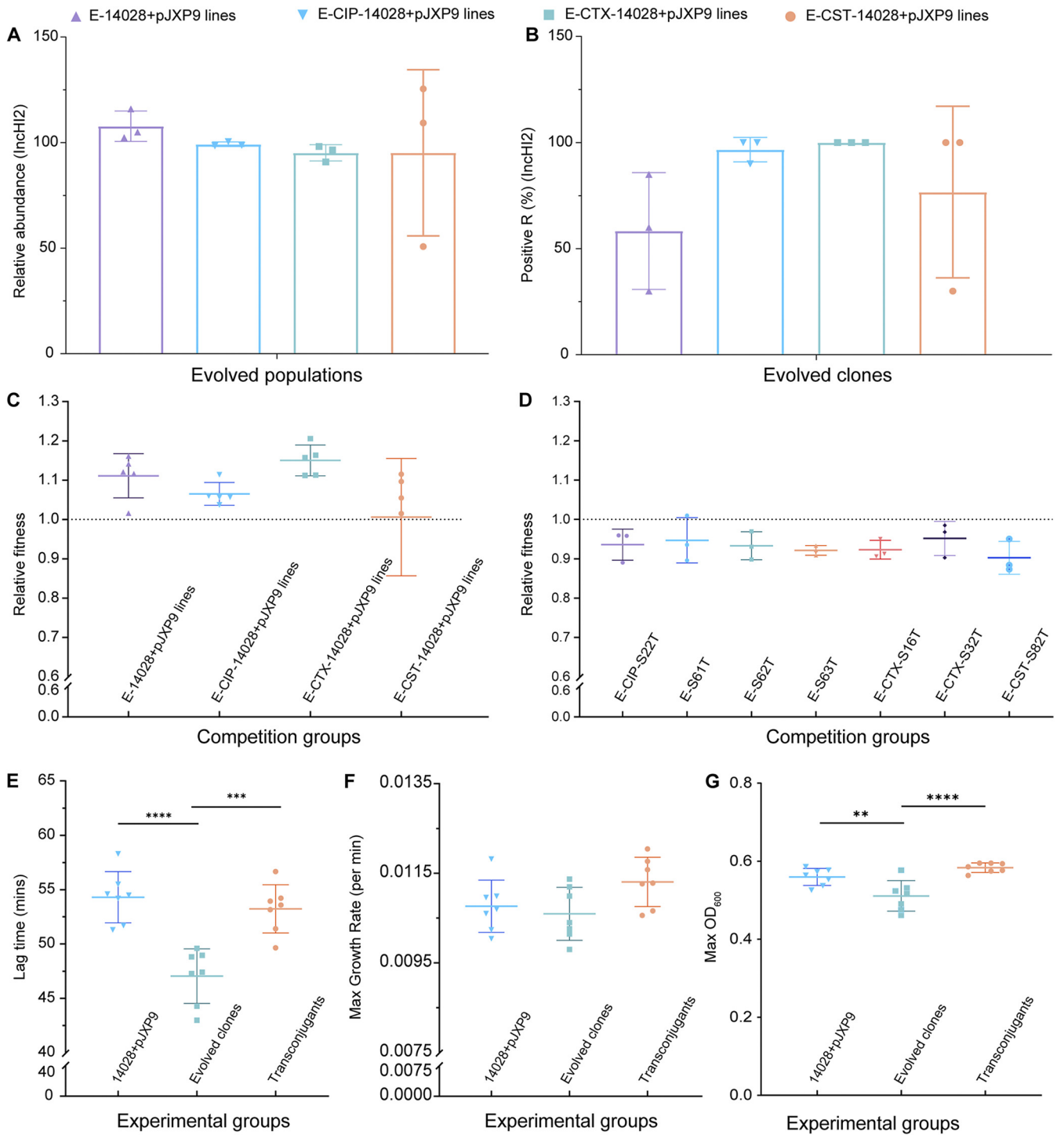


**FIG 1** Percentage abundances of *repH12* gene and fitness costs of plasmid carriage in evolved populations and clones. (A) Relative abundance of *repH12* gene in evolved populations. (B) Detection of *repH12* gene in evolved clones. (C) Relative fitness of 20 evolved ATCC 14028 clones bearing evolved pJXP9 versus ATCC 14028:*lux*+pJXP9 by competition assays. (D) Relative fitness of 7 ancestral ATCC 14028 clones bearing evolved pJXP9 (transconjugants) versus ATCC 14028:*lux*+pJXP9 by competition assays. (E to G) Lag time (E), growth rates (F), and culture density (max OD<sub>600</sub> values) (G) were calculated for 7 evolved clones bearing evolved pJXP9, corresponding transconjugants, and ATCC 14028:*lux*+pJXP9. All data from at least three biological replicates are presented as the mean ± SD, and the significance was determined by nonparametric one-way ANOVA (\*,  $P < 0.05$ ; \*\*,  $P < 0.01$ ; \*\*\*,  $P < 0.001$ ; \*\*\*\*,  $P < 0.0001$ ).

**Gene relative abundance is reduced in plasmid MDR and conjugative transfer regions in evolved populations.** We further determined the relative abundance in evolved IncHI2 plasmid pJXP9 by using the WGS data for 12 endpoint evolved populations under different treatments compared with ancestral plasmid pJXP9 populations.

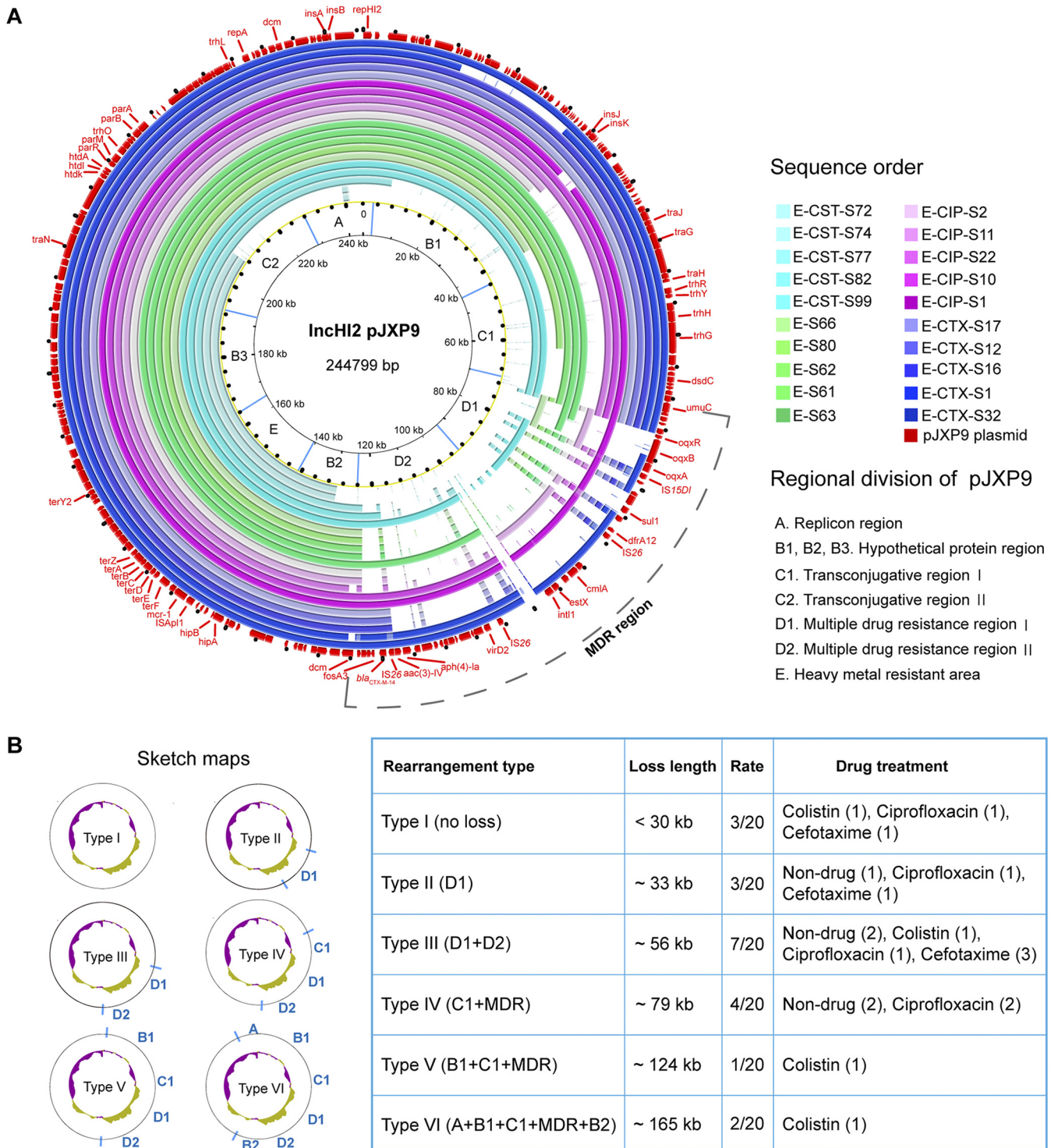


**FIG 2** Sequence analysis of endpoint evolved pJXP9 plasmids. (A) Circular sequence alignment of 20 evolved pJXP9 plasmids from endpoint evolved clones with ancestral pJXP9 plasmid from this study created using the BLAST Ring Image Generator (BRIG). Colored circles from outside to inside correspond to the list (sequence order) in the legend. Regional division of pJXP9 is according to the function of genes in the ancestral pJXP9 plasmid. (B) Summary information of deletion profiles for endpoint evolved plasmid pJXP9 from 20 selected evolved clones.

We found that alterations had occurred primarily in the MDR regions between *umuC* and *dcm* (~56 kb), including MDR I containing *oqxAB* between *umuC* and *pJXP9-70* (~33 kb) (D1) and MDR II containing *floR*, *bla<sub>CTX-M-14</sub>*, and *fosA3* between *pJXP9-70* and *dcm* (~23 kb) (D2) (Fig. 3A and B). Notably, the relative abundance of MDR I and MDR

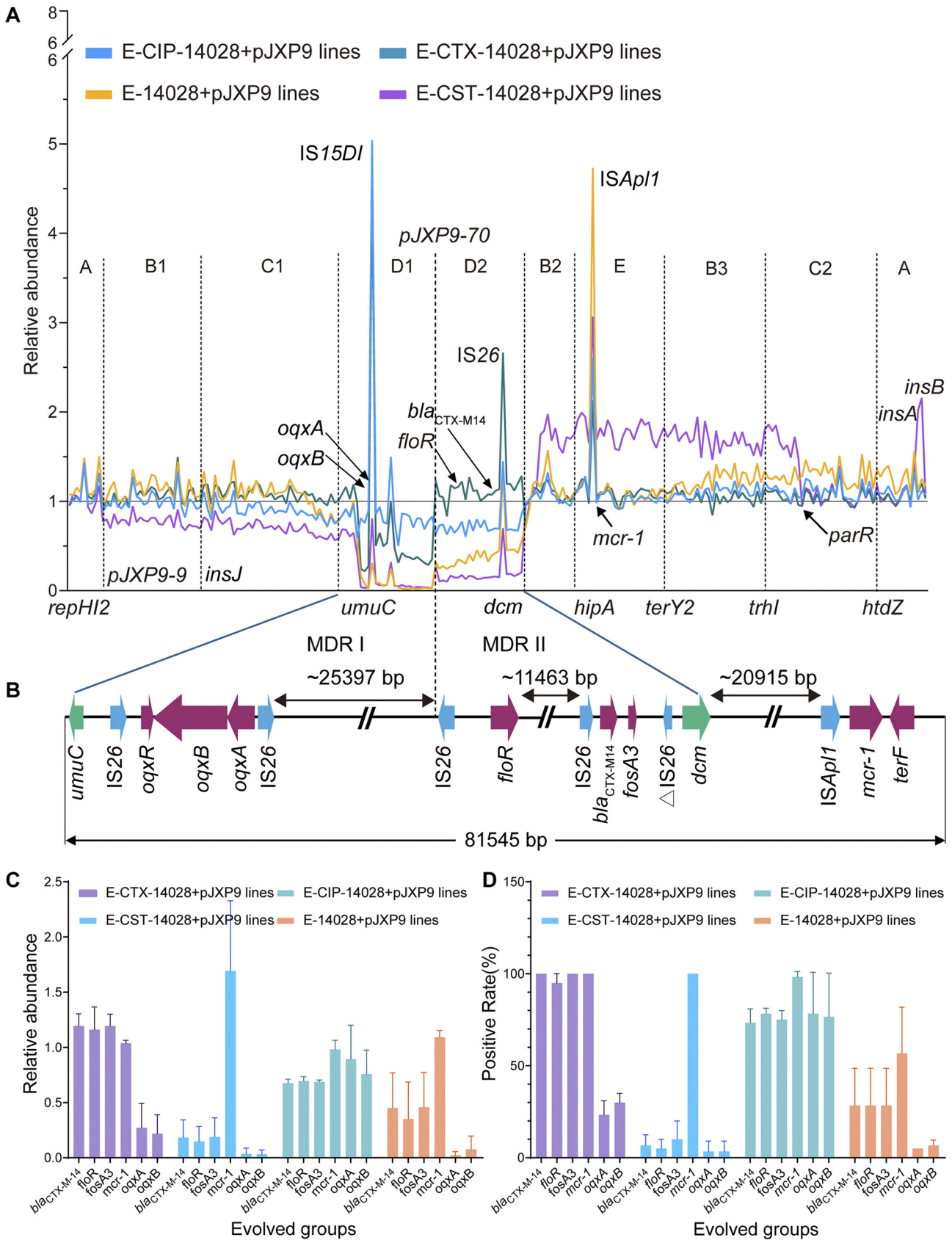


**FIG 3** Relative abundance of genes in plasmid pJXP9 from evolved populations under 4 experimental culture conditions. (A) Distribution of gene abundance in plasmid pJXP9 from endpoint evolved populations. (B) Characteristics of the MDR regions in ancestral pJXP9. (C) Relative abundance (Continued on next page)

II depended on the treatments: MDR I was retained at >60% with CIP and >25% with CTX, but gene loss was ~100% with CST and no antibiotic. In contrast, MDR II was retained at 100% with CTX, 65% with CIP, and 25% with no antibiotic and at 15% with CST. Regions (~85 kb, B2 + E + B3) containing *mcr-1*, *ter*-like genes, and hypothetical protein genes between *dcm* and *parR* largely increased in relative abundance to ~150% but declined to ~70% in region I containing the conjugative transfer region I (C1, ~38 kb) between *insJ* and *umuC* and a large hypothetical protein region (B1, ~56 kb) between *pJXP9-9* and *umuC* under CST treatment. Furthermore, relative abundances were slightly decreased to ~89% in the conjugative transfer region I (C1) under CIP treatment. However, the relative abundance was slightly increased to ~120% in the regions (~76 kb, between *terY2* and *insA/insB*) containing a hypothetical protein region (B3, ~23 kb) between *terY2* and *trhI* and the conjugative transfer region II (C2, ~36 kb) between *trhI* and *htdZ* in the absence of antibiotics (Fig. S4).

Additionally, gene relative abundances were largely increased for several insertion sequences, including IS15DI (containing 3 mutated codons compared with IS26) adjacent to *oqxA* and IS*Apl1* adjacent to *mcr-1* and IS26 adjacent to *bla*<sub>CTX-M-14</sub>. Intriguingly, the increased extent of gene relative abundance for these insertion sequences largely depended on treatment conditions. For example, the gene relative abundance of IS15DI was increased under CIP and CTX treatments, whereas IS*Apl1* relative abundance was largely increased in the absence of antibiotics, followed by that under CST, CIP, and CTX treatments. The gene relative abundances for IS26 increased under CTX, followed by that under CIP and no treatment. The gene relative abundance remained almost stable in the other regions or genes on evolved plasmids under different treatments compared with ancestral plasmid pJXP9-carrying populations. Taken together, these results were consistent with the sequence analysis of pJXP9 from endpoint evolved clones in which the MDR and conjugative transfer regions were frequently deleted in evolved plasmids and these deletions depended on antibiotic treatment conditions.

**The stability of clinically relevant ARGs carried by evolved plasmids was antibiotic treatment dependent.** The stability of clinically relevant ARGs in endpoint evolved clones and populations was further investigated using PCR (240 clones), qPCR (12 populations), and WGS (12 populations) analyses (Fig. 3C and D; Fig. S2). We found that the stability of *mcr-1*, *bla*<sub>CTX-M-14</sub>, *fosA3*, *oqxAB*, and *floR* was highly variable and differed between antibiotic treatments. Under CIP treatment, all five tested ARGs remained at high relative abundance, with detection rates of >70% and *mcr-1* abundance at ~100%. CTX treatment resulted in high abundance in all tested ARGs but *oqxAB*, which was retained at ~25%. Unexpectedly, under CST treatment, *mcr-1* was completely retained but all of the other four ARGs were almost completely lost at a rate of ~90% and *oqxAB* was lost at ~100%. Additionally, serial transfer in the absence of antibiotic selection resulted in retention of *mcr-1* at ~80%, followed by that of *bla*<sub>CTX-M-14</sub>, *fosA3*, and *floR* at ~45%. In contrast, *oqxAB* was almost completely lost (loss rate, ~95%). Antimicrobial susceptibility testing also indicated that resistance phenotypes of the 240 evolved clones were consistent with the presence of *oqxAB*, *mcr-1*, *bla*<sub>CTX-M-14</sub>, *fosA3*, and *floR* (Table S3). Taken together, these results indicate that similar to the MDR regions deletions, the stability of clinically relevant ARGs carried by evolved plasmids were also antibiotic treatment dependent.

**Different antibiotic treatments altered the trajectory of deletion mutations in evolved plasmids.** To determine the order of the large fragment deletion mutations in evolved plasmids, we investigated the temporal dynamics of pJXP9 and ATCC 14028 coadaptation evolution under ciprofloxacin and nondrug treatments by WGS using

### FIG 3 Legend (Continued)

for clinically important ARGs in endpoint evolved populations using population sequencing. (D) Detection rates of clinically important ARGs among endpoint evolved clones from evolved populations under 4 exposure conditions. All data were derived from at least 3 biological replicates and are presented as the mean ± SD, and levels of significance were determined by nonparametric one-way ANOVA (\*,  $P < 0.05$ ; \*\*,  $P < 0.01$ ; \*\*\*,  $P < 0.001$ ; \*\*\*\*,  $P < 0.0001$ ).

time series-evolved populations (days 1, 14, 28, 42, and 63) (Fig. S4). Under CIP exposure, genes in MDR I (excluding insertion sequences) were almost completely maintained and were stable across 63 serial passages, while those in MDR II (excluding insertion sequences) and C1 decreased to ~70% at day 63. Unexpectedly, the region containing *oqxR-oqxA-oqxB* and the class I integron harboring *aad1* (aminoglycoside resistance)-*cmIA* (chloramphenicol resistance)-*estX* (streptothricin acetyltransferase) were completely lost by day 42 and returned to the normal levels found in the ancestral population at day 63. In contrast, passages in the absence of antibiotics generated a gradual decline of MDR II that was slight at days 14 and 28 and more pronounced at days 42 and 63. MDR I also showed a slight decrease at days 14 and 28 and then decreased sharply at day 42 and was completely lost by day 63. Furthermore, the partial conjugative transfer region I (between *traJ* and *umuC*) showed slight decreases at days 42 and 63 (Fig. S4). Taken together, for pJXP9 populations evolved under CIP, the class I integration region and *oqxR-oqxA-oqxB* began to be deleted at least at day 42 and were then followed by deletions of MDR II and C1 by day 63. In contrast, for pJXP9 populations evolved under the absence of drug selection, large fragment deletions first occurred in MDR I and were then followed by deletions in MDR II and the partial conjugative transfer region I. Furthermore, the abundance of IS15DI (adjacent to *oqxA*), IS26 (adjacent to *bla<sub>CTX-M14</sub>*), and ISAp11 (adjacent to *mcr-1*) tended toward increasing, and the temporal dynamics was also observed under CIP and nondrug treatments.

**Mutations of chromosomal genes involved in the stress response contributed to the competition advantage of evolved hosts.** To analyze whether putative chromosomal modifications mitigate the fitness costs of pJXP9 plasmid carriage, we determined the complete genome sequences of 20 endpoint evolved clones, 12 endpoint evolved populations, and 2 ancestral clones as described above, as well as 8 controls (14,028 evolved clones/population). A total of 81 shared mutated chromosomal genes were identified after excluding mutations also found in the ancestral clones and controls. The mutations identified were common in 13 genes, with frequencies of  $\geq 45\%$  among both multiple evolved clones and populations. These genes were primarily associated with oxidative stress (*ahpC*, *ybgS*, *STM14\_1959*, and *STM14\_2022*), DNA repair (*umuC* and *alkB*), outer membrane permeability (*ompC*), osmotic stress (*osmY*), and sugar transporter (*yjiJ*), as well as hypothetical proteins (*STM14\_2712*, *STM14\_3239*, *STM14\_3253*, and *STM14\_4565*) (Fig. 4A and B). The gene *ahpC* encodes an alkyl hydroperoxide reductase subunit belonging to a two-cysteine peroxiredoxin family and is responsible for protecting cells from low concentrations of H<sub>2</sub>O<sub>2</sub> (11). The hypothetical protein YbgS containing two cysteine residues was probably associated with redox reactions (12). *STM14\_1959* and *STM14\_2022* encode a putative oxidoreductase and oxidase, respectively. These two genes act together with *ahpC* and *ybgS* as antioxidant-related genes, and inactivation of these genes most likely alters the ability of the oxidative stress response. AlkB is an alkylated DNA repair protein (13). DNA polymerase V subunit gene *umuC* is directly involved in the induction of mutagenesis and associated with the SOS response (14, 15). Mutations in these two DNA repair genes could enhance mismatch repair. The outer membrane porin C protein OmpC allows for ions and hydrophilic solutes to cross the outer membrane, and its mutation could lead to impairment of the structural integrity and change in the permeability of the outer membrane (13). Molecular chaperone OsmY is associated with osmotic shock and the growth state of bacteria (16–19), and mutation inactivation of this gene could impair osmotic stress and result in delayed growth compared with that of wild-type *S. Typhi* in SPI-2-inducing conditions (17). YjiJ is a putative sugar transporter, and its mutation might be associated with glucose metabolic disorders.

To directly test whether loss of gene function plays a role in ameliorating the cost of plasmid carriage, *ahpC*, *osmY*, and *ybgS* were selected, and knockout mutants of these genes were constructed in the ancestral ATCC 14028 background carrying ancestral and evolved plasmid pJXP9. We measured the fitness relative to the wild type with plasmid pJXP9. We found that with  $\Delta$ *ahpC*,  $\Delta$ *osmY*, or  $\Delta$ *ybgS*, ATCC 14028 mutants carrying ancestral plasmid pJXP9 had higher competitive advantages and slightly lower

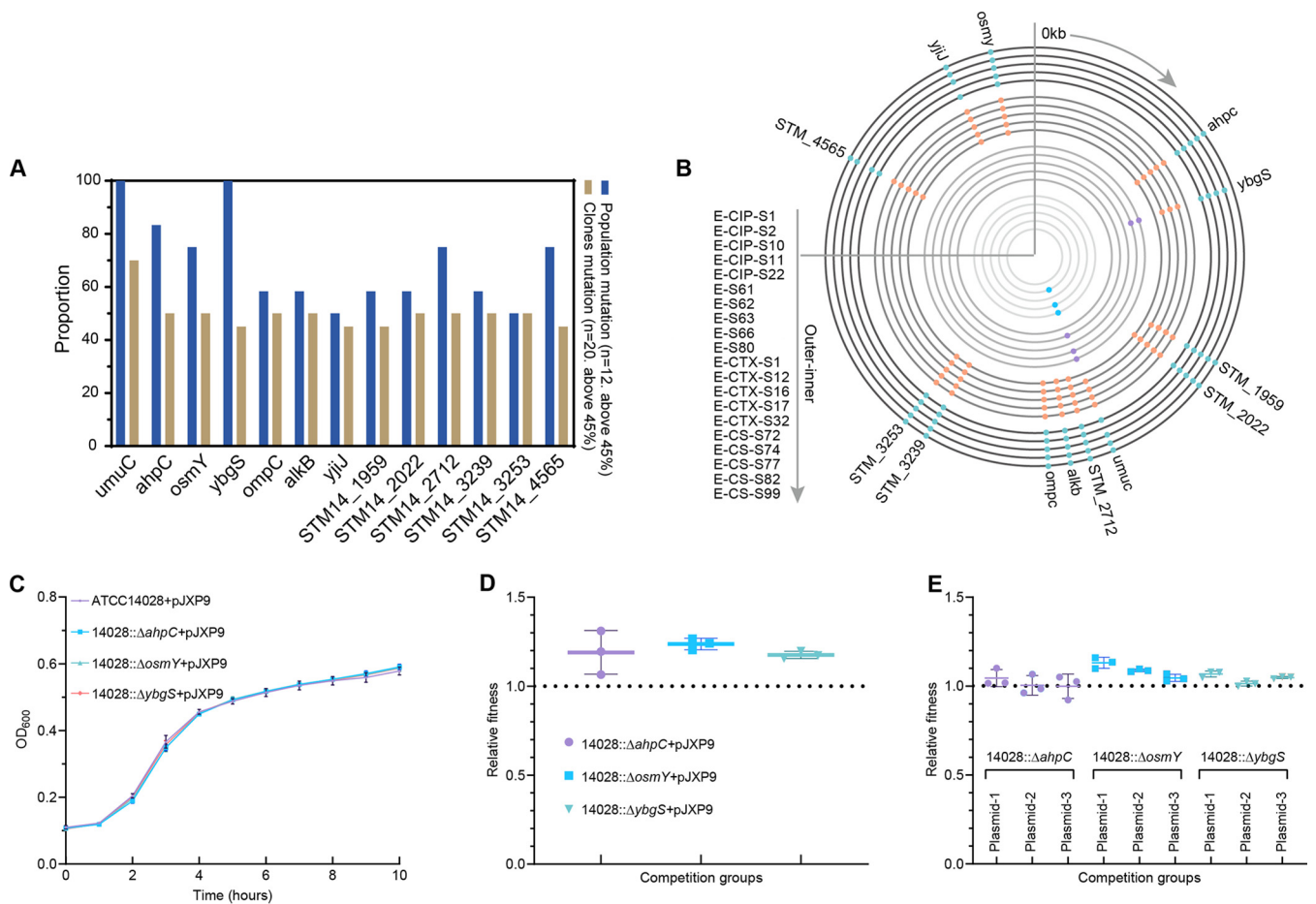


**FIG 4** Chromosomal compensatory mutation analysis and function verification. (A) Frequency analysis of compensatory mutations in chromosomal genes in populations and clones. Mutant frequencies were defined by numbers of occurrences in 12 evolved populations or 20 representative clones. The mutated genes also included mutations at different sites. Cutoffs were set at  $>0.45$ , because mutated genes were among the top 25% simultaneously in populations and clones.  $n$ , number of populations or individual clones used to detect mutations. (B) Mutants present in 20 evolved clones. Different colors represent different exposure conditions. (C) Growth curves for mutated ATCC 14028+pJXP9 and ancestral ATCC 14028+pJXP9 strains. (D) Relative fitness of mutated ATCC 14028+pJXP9 versus ATCC 14028::*lux*+pJXP9 strains. (E) Fitness estimation of mutated ATCC 14028 carrying evolved plasmid pJXP9 versus ATCC 14028::*lux*+pJXP9 strains. Plasmids 1 (from E-S62), 2 (from E-S63), and 3 (from E-CTX-S32) represent three types of evolved pJXP9 plasmids, respectively. All data were derived from at least 3 biological replicates and are presented as the mean  $\pm$  SD, and levels of significance were determined by nonparametric one-way ANOVA (\*,  $P < 0.05$ ; \*\*,  $P < 0.01$ ; \*\*\*,  $P < 0.001$ ; \*\*\*\*,  $P < 0.0001$ ).

growth rates than the ancestral strain ATCC 14028+pJXP9 (Fig. 4C and D). Furthermore,  $\Delta$ ahpC,  $\Delta$ osmY, or  $\Delta$ ybgS mutants carrying evolved pJXP9 also exhibited slightly higher competitive advantage than ancestral ATCC 14028+pJXP9 (Fig. 4E). This indicated that these gene deletions could generally alleviate the cost produced by possession of pJXP9 to some extent. Furthermore, multiple gene mutations were identified in endpoint evolved populations or clones that were under CIP or nondrug exposure (Fig. 4B). Taken together, adaptive coevolution of plasmid pJXP9 within *S. Typhimurium* ATCC 14028, particularly in the presence of CIP or with no drug, promoted the competitiveness of the evolved bacterial host through compensatory mutations in primarily stress response genes.

**Alterations in convergent gene mRNA abundance were related to impaired physiological functions in evolved bacterial hosts with rearranged pJXP9 plasmids.** Phenotype and genome analyses of evolved populations and clones indicated that the carriage costs of pJXP9 plasmid in *Salmonella* could be ameliorated through mutations in chromosomal genes associated with the stress response and large fragment deletions in the conjugative transfer regions and multidrug resistance regions in the plasmid. This suggested that there were convergent physiological responses to the

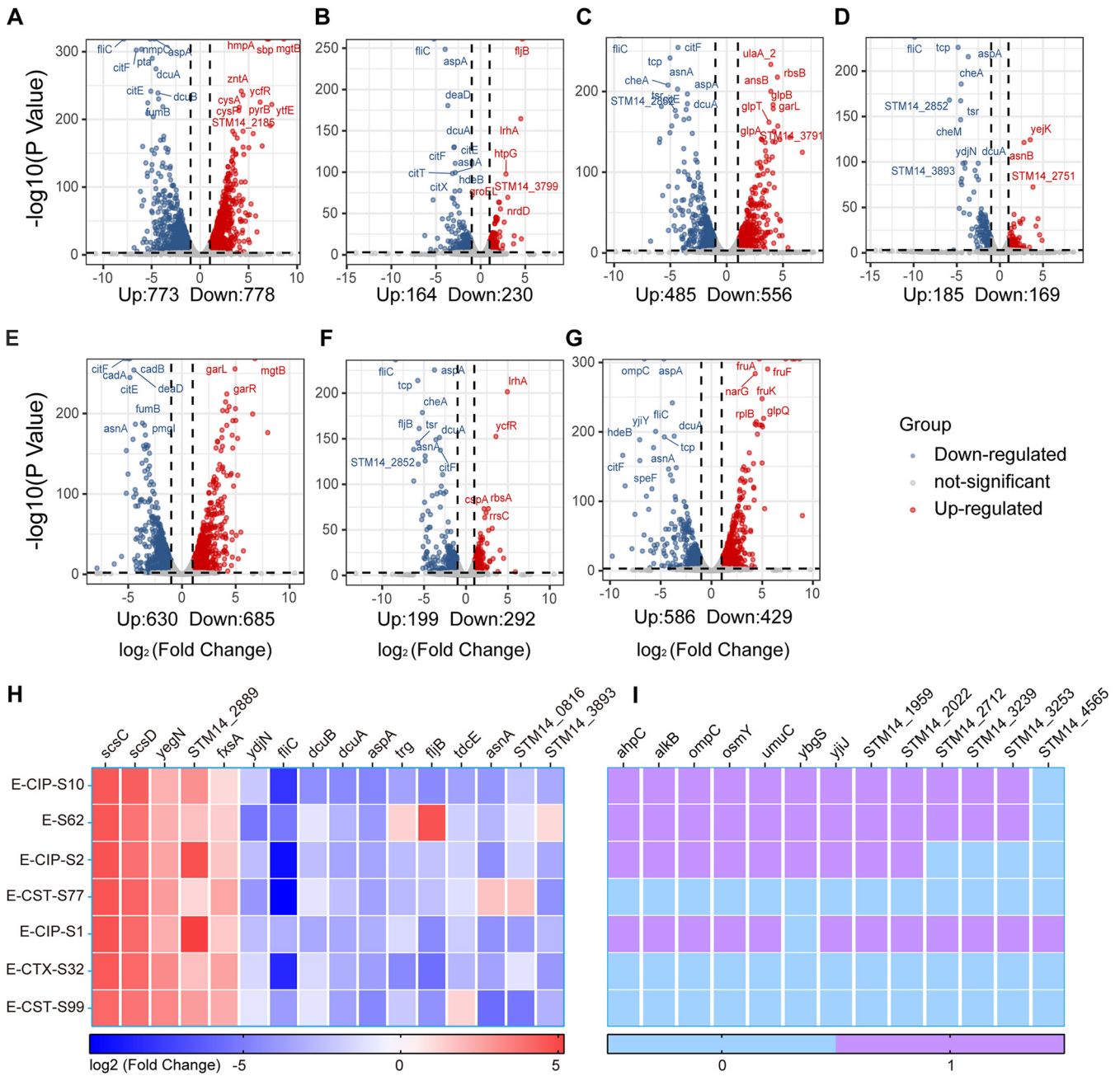


**FIG 5** Transcriptome profiles for 7 representative endpoint evolved clones relative to that of the ancestral ATCC 14028+pJXP9 without antibiotic pressure. (A) E-CIP-S10 (type II, D1 deletion); (B) E-S62 (type III, MDR region deletion); (C) E-CIP-S2 (type IV, MDR region + C1 deletion); (D) E-CST-S77 (type V, MDR region + B1 + C1 deletion); (E) E-CIP-S1 (type I, no loss); (F) E-CTX-S32 (type I, no loss); (G) E-CST-S99 (type I, no loss). The 7 endpoint evolved clones were selected based on the deleted regions of evolved plasmid pJXP9 in Fig. 2. The colored points define significant (\*\*\*,  $P < 0.001$ ) differential expression (>2-fold change). Points represent upregulated genes (light red), downregulated genes (light blue), and not-significant genes (gray), respectively. (H) Shared up- or downregulated genes in seven evolved isolates. (I) Shared mutated genes in seven evolved isolates.

carriage of and compensation with this plasmid. To understand these responses and their resolution, we performed RNA sequencing (RNA-seq) on endpoint evolved isolates carrying nearly complete plasmid pJXP9 (3 isolates) and incomplete ones with different deleted regions, from ~33 kb to ~165 kb (4 isolates) (Fig. 5A to G), with or without chromosomal amelioration mutations (Fig. 5I). The pJXP9 plasmid-carrying ancestral clone was chosen as a control. In these 7 evolved isolates, chromosomal gene expression was altered, and the numbers of significantly upregulated and downregulated genes ranged from 185 to 773 and from 169 to 778, respectively (Fig. 5A to G). Furthermore, the

number of significantly downregulated genes was slightly higher than that of upregulated genes in 5/7 evolved isolates. The opposite situation was observed in the remaining 2 isolates (Fig. 5D and G). Notably, a set of 16 shared chromosomal differentially expressed genes (DEGs) were identified in all of these 7 evolved clones. These included 5 upregulated genes (*scsC*, *scsD*, *yegN*, *STM14\_2889*, and *fxsA*) and 5 downregulated genes (*ydjN*, *fliC*, *dcuB/dcuA*, and *aspA*), as well as 6 genes that were up- or downregulated in different evolved isolates (Fig. 5H). *AspA* is linked to the tricarboxylic acid (TCA) cycle and aspartate metabolic pathways and catalyzes the conversion of fumarate to L-aspartate (20). *dcuA/dcuB* encodes common C4-dicarboxylate/aspartate transporters that are active under anaerobiosis (20, 21). The downregulation of these 3 genes (*AspA*, *dcuA* and *dcuB*) indicated that aspartate metabolic pathways might be inhibited. Interestingly, the fimbrial gene *fliC*, which encodes a structural flagellar protein (22), was downregulated, and this would reduce flagellar motility. *YdjN* functions as a transporter of S-sulfo-cysteine, a sulfur-containing intermediate in assimilatory cysteine biosynthesis (23), and its downregulation might impair cystine metabolism and oxidative stress responses (24). *scsABCD* encode 4 proteins in *Salmonella* that resemble the disulfide folding machinery of other bacteria, and upregulation of *scsBC* is linked to adaptation to Cu and H<sub>2</sub>O<sub>2</sub> stress (25). *yegN* is part of a tripartite efflux system, and its deletion results in decreased growth (26). *FxsA* overproduction in *Escherichia coli* inhibits the F plasmid-mediated exclusion of bacteriophage T7 and interacts with the F plasmid-encoded PifA protein to minimize membrane damage (27).

Our transcriptome data from evolved plasmid pJXP9, which remained intact from evolved isolates E-CIP-S1, E-CTX-S32, and E-CST-S99, revealed that plasmid-borne genes located on the conjugative transfer regions (C1 and C2) were almost all downregulated except for *parAB* and *parMR*. Almost all of the MDR genes were upregulated, with a few exceptions (Fig. S5). Of note, the corresponding resistance phenotypes in these three clones were almost not changed (Table S3). Taken together, the gene expression alterations in sets of shared chromosomal and plasmid-borne genes in the endpoint evolved clones would most likely result in impaired fumaric acid synthesis, flagellar motility, and antioxidant activity, as well as decreased conjugation and bacteriophage-mediated horizontal gene transfer but enhanced resistance against copper.

## DISCUSSION

IncHI2 plasmids are relatively large (>200 kb), and how they are successfully maintained or persist in the bacterial host is unknown, in particular in *S. Typhimurium*. We found that the fitness cost imposed on *S. Typhimurium* ATCC 14028 by IncHI2 plasmid pJXP9 carriage was partially alleviated through coculture of IncHI2 plasmids and *S. Typhimurium* ATCC 14028. Specifically, experimental evolution was performed for hundreds of generations to achieve potential mutation or fitness-improved information (28). These compensatory mutations included deletions in the plasmid MDR and conjugative transfer regions and specific hypothetical protein regions in evolved plasmids (Fig. 6). Interestingly, these changes were dependent of the presence and type of antibiotic, and similar scenarios of large plasmid MDR region deletions have been reported for evolved plasmid pKP33 in *Klebsiella pneumoniae* and evolved plasmid pUR2940 in *Staphylococcus aureus* lineages (5, 29). Indeed, these deletions that we found in the MDR region enhanced the growth rate of transconjugants compared with that of ancestral pJXP9-carrying clones. Furthermore, the evolved isolates E-CIP-S1, E-CTX-S32, and E-CST-S99 carried evolved plasmid pJXP9 without any large fragment deletion, while almost all gene expression from transconjugative regions I and II were downregulated except for that of *parAB* and *parMR* (see Fig. S5 in the supplemental material). Conjugation is energetically expensive for host cells, and impairing conjugative transfer probably benefits plasmid maintenance in the bacterial host (30). *parAB* and *parMR* are inserted into the transfer gene clusters and capable of supporting partitioning in IncHI2 plasmids (31), and since these genes were not downregulated, their expression most likely facilitated plasmid partitioning and maintenance in the bacterial

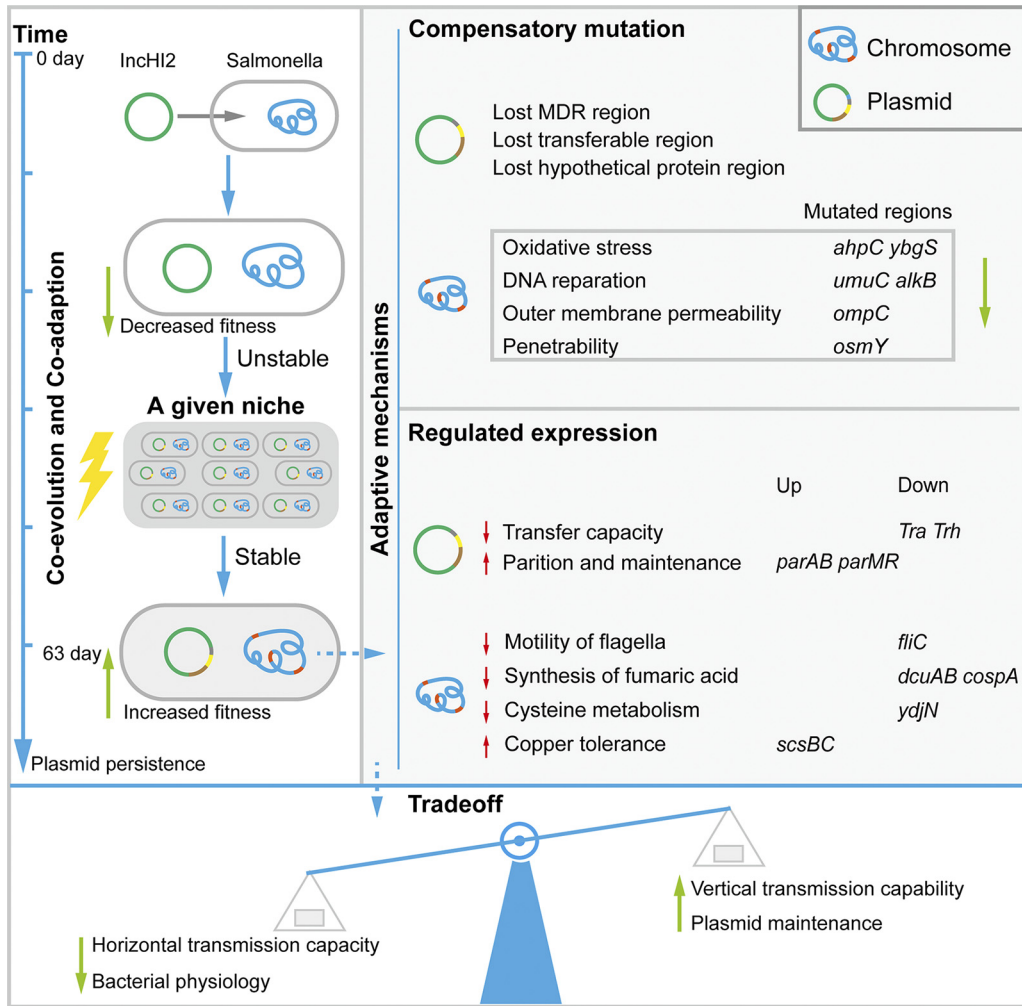


**FIG 6** Possible mechanisms underlying adaptive evolution of the IncHI2 plasmid pJXP9 and bacterial host *Salmonella* Typhimurium ATCC 14028.

host. However, unexpectedly, increased expression of MDR genes was observed on evolved plasmid pJXP9 from evolved isolates E-CIP-S1, E-CTX-S32, and E-CST-S99, although MDR region deletions were also common in other evolved clones or evolved populations. This process was most likely linked to an increase in survival ability under antibiotic exposure. Taken together, the conjugation transfer and MDR regions seemed to be one of the primary factors that exerted fitness costs on carriage of IncHI2 plasmids while adaptive plasmid evolution includes deletions that promoted host bacterial growth while retaining the plasmid.

We also identified numerous parallel compensatory mutations that appeared in evolved plasmids that included many types of fragment deletions, and interestingly, the extent and range of these deletions on the plasmid in endpoint evolved populations could be linked to culture conditions. Similarly, the differentiated trajectory of deletion mutations in evolved plasmids was also found to be related to selection pressure during the serial evolutionary process under ciprofloxacin and nondrug exposure. But the reasons why gene abundance and deletion mutations occurred between drug exposure groups at specific times remain unclear. One possible explanation is that insertion sequences (ISs) most likely were the arbiters of fragment deletion and recombination (29, 32), and this was reflected in the high gene relative abundance of IS elements in evolved populations. This was especially true for *oqxAB*, *bla<sub>CTX-M14</sub>*, and *mcr-1* under corresponding antibiotic treatment conditions. Indeed, ISs contribute to ARG transmission in response to antibiotic exposure and are involved in plasmid-bacterium coadaptation

(33–35). Taken together, these results illustrated the dynamics and complexity of plasmid-bacterium coadaptation and coevolution under different antibiotic treatments and time points. The ISs played a significant role in IncHI2 plasmid evolution. Specific parallel compensatory mutations or mutation trajectories were probably due to the directional selection of specific treatments with time, and it made plasmid carriage advantageous.

In addition to compensatory deletion mutations in evolved plasmids, bacterial hosts have evolved diverse chromosomal compensatory mutations, such as the global regulatory system genes *gacA/gacS*, the DNA helicase genes *uvrD* and *xpd/rad3*, the nonselective outer membrane porin gene *ompF*, the efflux pump genes *acrAB/acrR*, and PFLU4242 of unknown function (36–39). We found a series of chromosomal mutations in stress response genes in evolved clones and, in particular, under CIP exposure or the lack of a drug. We identified deletions in oxidative stress-associated genes, such as the alkyl hydroperoxide reductase gene *ahpC* and other related but uncharacterized genes (*ybgS*, *STM14\_1959*, and *STM14\_2022*) and genes for DNA repair (*umuC* and *alkB*), outer membrane permeability (*ompC*), and osmotic stress (*osmY*). The deletions of *ahpC*, *osmY*, and *ybgS* in the ancestral ATCC 14028 background carrying plasmid pJXP9 improved the competitive capacity of the host. Furthermore, other downregulated genes were independent of antibiotic exposure and were related to bacterial physiological functions, including impaired flagellar motility (*fliC*), blocked fumaric acid synthesis (*dcuB/A* and *aspA*), decreased resistance to oxidative stress (*ydjN*), inhibited bacteriophage-mediated horizontal gene transfer (*fxsA*), and enhanced Cu resistance (*scsCD*). Plasmid acquisition is often associated with reduced bacterial motility and is sometimes due to downregulation of flagellar genes (40). In this study, the swimming zones were significantly inhibited in endpoint evolved strains compared to those of ancestral strains that carried pJXP9 ( $P < 0.01$ ), whereas the swimming zones in transconjugants carrying evolved plasmids were restored and comparable to those of ancestral strains with ancestral pJXP9 (Fig. S6; see also Text S1 in the supplemental material). These data indicate that impaired flagellar motility was most likely the result of the evolved chromosome. This also implied that potential conflicts between plasmid-bearing and chromosomal genes were also a significant source of fitness cost of carrying pJXP9. As a result, both chromosomal compensatory mutations and altered chromosomal expression profiles influenced bacterial physiology phenotypes to reduce plasmid-carrying costs through coevolution. These indicated that plasmid fitness costs caused by specific genetic conflicts are unlikely to act as a long-term barrier for the persistence of plasmids (36). Furthermore, plasmids can also manipulate chromosomal gene expression (40). Therefore, further studies are required to determine how adaptive coevolution links these bacterial phenotypes to plasmid fitness.

There are other ecological and evolutionary solutions to the plasmid paradox besides compensatory evolution (41). For example, chromosomal adaptive mutations controlling the global regulatory systems for carbon catabolite repression (CCR) and anaerobic metabolism (ArcAB) reduced the fitness cost of MDR plasmid carriage in specific bacterial niche adaptations (42). Furthermore, bacterial communities that contain multiple species can act as surrogate hosts to maintain a plasmid in the population (42). Moreover, an additional explanation for the maintenance of conjugative plasmids has been proposed, i.e., that plasmid donor cells can also be effective competitors with plasmid-free cells particularly in structured environments (28). Further study is required to determine whether other ecological and evolutionary mechanisms of plasmid stability, such as piggybacking on niche adaptation, can alter the maintenance of IncHI2 plasmids in *S. Typhimurium*.

This study proposes that the source of fitness costs of transferable MDR IncHI2 plasmids depends on plasmid gene expression as well as conflicts between these regions and the chromosome. As a result, compensatory plasmid-borne and chromosomal mutations and altered chromosomal expression profiles collectively contributed to alleviating the fitness costs during adaptive coevolution of the plasmid and the host bacterium. Of note, this adaptive coevolution is also a trade-off between improved

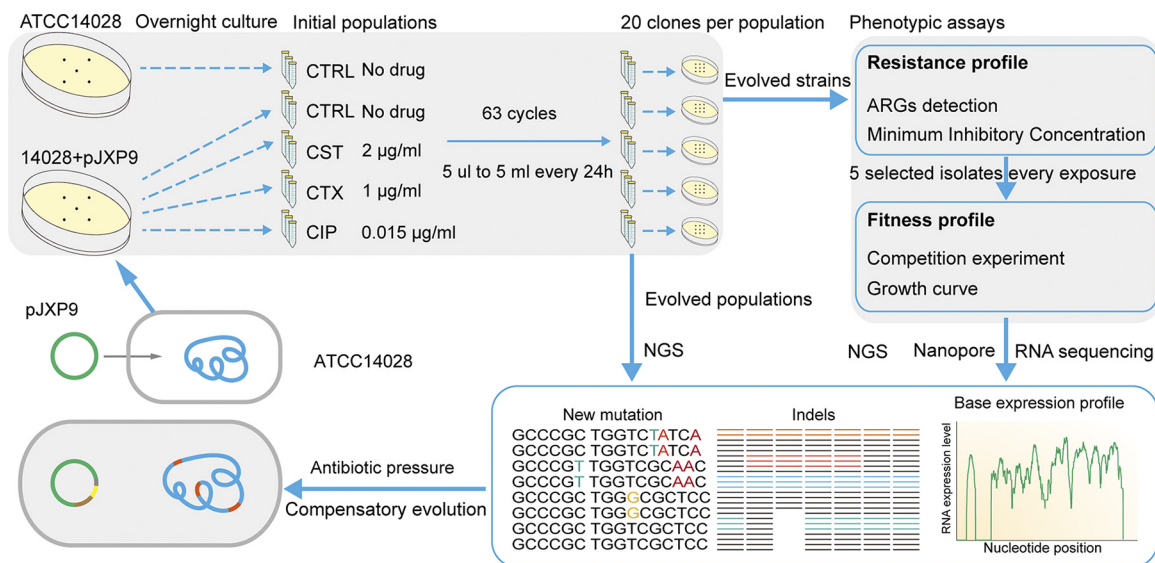


**FIG 7** Schematic overview for adaptive evolution of plasmid-bacterial host under subinhibitory or nondrug exposure. Colonies taken from LB agar plates of ancestral clones ATCC 14028+pJXP9 and ATCC 14028 were picked and inoculated into fresh LB broth as initial cultures and serially passaged in triplicate for 63 days. Twenty clones from each evolved population were selected for MICs and ARG detection, and representative clones ( $n = 5$ ) were selected for estimating plasmid fitness effects by competition assays and growth curves. Evolved populations and evolved clones were further submitted to WGS by Illumina. Nanopore sequencing was also performed for representative clones harboring evolved IncHI2 plasmids of different sizes. Furthermore, evolved clones carrying plasmids of different sizes were subjected to whole-genome RNA sequencing. Parallel mutations for evolved populations and clones and mRNA abundance alterations were analyzed.

growth and competitiveness, with impairments in bacterial physiological processes such as flagellar motility, horizontal gene transfer, cell membrane permeability, fumaric acid synthesis, and resistance to oxidative and osmotic stress. Considering that the specifics of evolutionary dynamics likely vary with the environment and organism, further studies are still required to reveal the nature of adaptive evolution of plasmids and bacteria.

## MATERIALS AND METHODS

**Strains and experimental evolution.** The plasmid pJXP9 (~244 kb) was derived from an *E. coli* J53 transconjugant of *S. Typhimurium* JXP9 recovered from a pig in Jiangxi, China, in 2017, possessed a typical IncHI2 plasmid backbone, and carried at least 15 ARGs, including *mcr-1*, *bla*<sub>CTX-M-14</sub>, *fosA3*, *oqxAB*, and *floR* (9). The plasmid pJXP9 was introduced into *S. Typhimurium* ATCC 14028 by conjugation, and transconjugants were defined as the initial ancestral strain (denoted ATCC 14028+pJXP9) and used for experimental evolution (for details, see Text S1 in the supplemental material). Briefly, cultures were grown in 5 mL Luria Bertani (LB) broth in 50-mL tubes at 37°C and shaken at 180 rpm. Independent selection lines were founded using 12 independent single colonies of ATCC 14028+pJXP9 taken from plate cultures, grown overnight in LB in the absence of antibiotics (nonselective conditions), and split into four exposure groups with biological triplicates: (i) no antibiotic selection, (ii) 2 µg/mL colistin (CST), (iii) 1 µg/mL cefotaxime (CTX), and (iv) 0.015 µg/mL ciprofloxacin (CIP). In parallel, three independent ATCC 14028 colonies were picked up for control treatments and grown in the absence of selection. Cultures were serially diluted 1/1,000 every consecutive day (24 h) for 63 days ( $63 \times \log_2 1,000$ ) to achieve ~627.8 generations calculated as previously described (28, 43). The final tally for these experiments was 15 endpoint evolved populations (5 exposure scenarios and biological triplicates for each exposure) and a total of 300 endpoint clones (20 clones were selected randomly from each evolved population), which were stored in 30% glycerol at -80°C and used later for phenotyping, whole-genome sequencing (WGS), and RNA sequencing (Fig. 7). Additionally, evolved populations derived from days 1, 14, 28, and 42 that included 3 populations had been passaged in the absence of antibiotics, and 3 populations in the presence of CIP were also stored at -80°C and further deep sequenced (see below).

**Plasmid stability, ARGs, and MIC detection.** The stability of pJXP9 and its ARG content were determined at the end of the selection experiment using PCR screening of 20 randomly picked colonies from each tested endpoint population (240 total) using primer sets specific for the plasmid genes *repH12*, *mcr-1*, *bla*<sub>CTX-M-14</sub>, *oqxAB*, *fosA3*, and *floR* (Table S1). Plasmid drug resistance was assessed by determining the MICs for 6 antibiotics, including colistin (CST), florfenicol (FFC), cefotaxime (CTX), fosfomycin (FOS), ciprofloxacin (CIP), and nalidixic acid (NAL), in the selected colonies (total, 300 endpoint clones), and the results were interpreted according to the CLSI and veterinary CLSI guidelines (44, 45). MICs for FOS were

determined using Mueller-Hinton agar supplemented with 25  $\mu\text{g/mL}$  glucose-6-phosphate. *Escherichia coli* ATCC 25922 served as the quality control strain.

The relative abundances of the 6 plasmid target genes in endpoint populations were determined using quantitative real-time PCR (qPCR) as previously described (2). Briefly, total DNA was extracted from evolved and ancestral pJXP9-bearing populations that were grown in LB broth at 37°C for 10 h. qPCR assays were performed in triplicate using the primers listed in Table S1. The 16S rRNA gene was used as an internal control for DNA quantification. Relative quantification was calculated using the  $2^{-\Delta\Delta C_T}$  method (46) [ $\Delta\Delta C_T = (C_{T, \text{target}} - C_{T, \text{control}})_{\text{evolved populations}} - (C_{T, \text{target}} - C_{T, \text{control}})_{\text{ancestral populations}}$ ].

**Growth curves and competitive fitness assays.** Growth curves and competition assays are frequently used methods for estimating plasmid fitness effects (47). Growth curves were measured using triplicate overnight cultures that were diluted to an  $\text{OD}_{600}$  of 0.1 in LB broth and distributed in 96-well plates at 200  $\mu\text{L}$  per well. The assay plates were placed into an EnSight multimode plate reader (PerkinElmer, USA) and incubated at 37°C with continuous shaking at 180 rpm, and growth was recorded by measuring the optical density ( $\lambda = 600 \text{ nm}$ ) for a minimum of 10 h. These data were used to extract parameters that served as proxies for bacterial fitness: (i) maximum growth rate (estimating the intrinsic population growth rate), (ii) maximum optical density (max  $\text{OD}_{600}$ , carrying capacity), and (iii) lag phase duration (lag time, defined as the integrated time lost during adaptation to new conditions compared with an immediate response) (48, 49). Data were processed using the Growthcurver package in R (50). Growth curves were also constructed for ancestral strain ATCC 14028 and ATCC 14028+pJXP9 as well as for endpoint clones bearing evolved plasmid (for details, see Text S1).

The relative fitness (RF) of plasmid-carrying versus plasmid-free clones or ancestral plasmid-carrying versus evolved plasmid-carrying clones was estimated using direct *in vitro* competition assays in triplicate as previously described with slight modifications (51). In brief, growth competition was initiated using a strain cultured for 24 h in LB medium at 37°C and then diluted to an  $\text{OD}_{600}$  of 0.1, mixed in a 1:1 ratio, incubated at 37°C for 24 h (day 1), and then diluted to obtain separate colonies when plated on LB agar containing 2  $\mu\text{g/mL}$  CTX or no antibiotic to obtain CFU. Competition assays using ancestral ATCC 14028 versus the ancestral pJXP9-bearing ATCC 14028 strain were performed for 7 consecutive days following the described methods. Competition assays of evolved ATCC 14028 strains bearing the evolved pJXP9 versus ATCC 14028:*lux*+pJXP9 and of ancestral ATCC 14028 bearing the evolved plasmid versus ATCC 14028:*lux*+pJXP9 were performed in 1 day. Colonies were screened for epifluorescence using a Leitz Aristoplan microscope and compared to the total plate CFU. The relative fitness was calculated using the equation  $\text{RF} = (\log_{10} S1_{dt} - \log_{10} S1_{d0}) / (\log_{10} S2_{dt} - \log_{10} S2_{d0})$ , where  $S1$  and  $S2$  represent CFU densities of two tested clones ( $t = \text{time in days}$ ),  $d0$  and  $dt$  represent the time when CFU densities of clone  $S1$  or clone  $S2$  were determined respectively (51). An RF of  $>1$  indicated a selective advantage over the control strain, whereas an RF of  $<1$  represented a fitness cost.

**Genome sequencing and plasmid analysis.** Representative evolved clones were sequenced based on MIC and PCR results. Genomic DNA was extracted using a Genra Puregene bacterial DNA purification kit (Qiagen, Hilden, Germany) according to the manufacturer's instructions. The DNA was sequenced using an Illumina HiSeq platform (Novogene, China), and sufficient sequencing depth ( $>100$ ) was obtained for further analysis (1 Gb per clone and 6 Gb per population). The raw data of genomes were filtered by Trimmomatic with -phred 33 (v 0.32), and the clean data were assembled to calculate the estimated genome change using SPAdes (v3.6.2) (-t 30 -k 21,33,55,77,99,127 -careful -phred-offset 33) (52) (Table S2).

High-quality reads were mapped to the plasmid pJXP9 sequence using SOAP aligner/SOAP2 with a maximum alignment error of 5 (53). The relative gene abundances of evolved plasmids (all genes in pJXP9) from evolved populations for transfers at days 1, 14, 28, 42, and 63 were normalized using RPKM (reads per kilobase per million reads) with ancestral pJXP9 as the reference (54). Alignments between evolved plasmids and ancestral plasmids and generation of circular maps were performed using BRIG (v 0.95) (55). Nanopore sequencing was further conducted to obtain the complete nucleotide sequence of plasmid pJXP9 in endpoint evolved clones. For clones sequenced by Nanopore and Illumina, sequence assembly was performed using Unicycler using default parameters for hybrid assembly (v 0.4.8) (56). Plasmid size and GC content alterations for evolved chromosome and plasmid were compared with those of ancestral references using Snapgene (v5.0). The sizes of IncHI2 plasmids were measured from 2 ancestral and 20 evolved strains after linearization of genomic DNA using S1 nuclease (TaKaRa, Dalian, China) by pulsed-field gel electrophoresis (PFGE), followed by Southern blotting hybridization using a digoxigenin-labeled probe specific for *repHI2* (Table S1) as previously described (57) (for details, see Text S1).

**Mutation analysis and function verification.** Sequencing reads of endpoint ATCC 14028+pJXP9 evolved populations and clones were mapped to the ATCC 14028 reference genome (accession no. CP001363 downloaded from <https://www.ncbi.nlm.nih.gov/nucleotide/CP001363/>), and basic variants were called using the CLC Genomics Workbench 10.0 (Qiagen, Hilden, Germany) with default parameters (basic variant detection, similarity fraction of 0.9, minimum coverage of 100, minimum count of 10, and minimum frequency of 10.0%). All chromosomal mutations occurring in  $>10\%$  of the reads and in at least 10 unique reads were included in the analysis, while those occurring in noncoding regions were excluded (58, 59). Then, the mutations that were present in corresponding endpoint ATCC 14028 evolved populations and clones were filtered out from the above-described mutation results. To better reflect the origin of mutation among populations and clones, we clustered different mutations into the corresponding genes using the following rules: (i) mutations that occurred in  $>10\%$  in either evolved populations or clones were defined as valid and (ii) cutoffs for gene mutation frequencies among evolved populations and clones were set to acquire the top 25% of the mutated genes.

To confirm the impact of chromosomal gene mutation on fitness cost of pJXP9 plasmid carriage, the selected target genes were deleted in ancestral strain ATCC 14028 bearing plasmid pJXP9/evolved plasmid

pJXP9 by use of the two-plasmid system pCaspA-pSGKp (based on CRISPR/Cas9-mediated genome editing) CRISPR-Cas9 methods as described in Text S1. The designed 20-nt base-pairing region (N20) of sgRNA for deleting targeted genes and primers for detecting fragment deletion are listed in Table S1. Growth curves and competitive fitness assays were performed among the mutation strains as described above.

**Whole-genome RNA sequence analysis and bioinformatics.** In order to analyze the gene expression levels of endpoint evolved clones with evolved plasmid, RNA was extracted from the selected clones cultured in LB broth for 4 h without antibiotics as previously described (60, 61). Bacterial cells were collected by centrifugation at  $8,000 \times g$  for 10 min. The library was constructed using an Illumina TruSeq RNA sample prep kit v2 as previously described (62) and sequenced using the Illumina HiSeq 2000 platform. High-quality reads that passed the Illumina quality filter with Trimmomatic -phred 33 were mapped to the *S. Typhimurium* strain ATCC 14028 genome using the FANSe 2 algorithm with parameters -L55 -E2 -U1 -S10. Genes with  $\geq 10$  mapped reads were considered confidently detected genes. Gene expression levels were estimated using RPKM (reads per kilobase per million reads) (54). Gene differential expression analysis was performed as previously described (63). The genes with a  $< 0.001$  false discovery rate (FDR) and a change of  $> 2$ -fold or  $< 0.5$ -fold were detected as differentially expressed genes (DEGs).

**Statistical analyses.** Statistical analyses were performed using Prism 8.0 (GraphPad, San Diego, CA, USA). All data were obtained from at least three biological replicates and are presented as the mean  $\pm$  standard deviation (SD). Unpaired Student's *t* test (nonparametric) between two groups and one-way analysis of variance (ANOVA) (nonparametric) among multiple groups with a *post hoc* test were used to calculate *P* values. Significance levels are indicated as follows: \*,  $P < 0.05$ ; \*\*,  $P < 0.01$ ; \*\*\*,  $P < 0.001$ ; and \*\*\*\*,  $P < 0.0001$ .

**Additional material.** Supplementary figures that support the findings in this research were submitted to the figshare database (<https://doi.org/10.6084/m9.figshare.20416359>).

**Data availability.** The population sequencing data and RNA sequencing data reported in this paper have been deposited in the NCBI SRA and GEO databases (BioProject accession no. [PRJNA810373](https://www.ncbi.nlm.nih.gov/bioproject/PRJNA810373) and [PRJNA810452](https://www.ncbi.nlm.nih.gov/bioproject/PRJNA810452) and GEO accession no. [GSE197475](https://www.ncbi.nlm.nih.gov/geo/query/acc.cgi?acc=GSE197475)), respectively. Complete sequences of the evolved strains sequenced by Nanopore and Illumina have been deposited in the GenBank database under accession numbers [SAMN26490219](https://www.ncbi.nlm.nih.gov/nuccore/SAMN26490219) to [SAMN26490228](https://www.ncbi.nlm.nih.gov/nuccore/SAMN26490228). All other data related to this study are available upon request.

## SUPPLEMENTAL MATERIAL

Supplemental material is available online only.

**TEXT S1**, DOCX file, 0.03 MB.

**FIG S1**, TIF file, 0.7 MB.

**FIG S2**, TIF file, 1.2 MB.

**FIG S3**, TIF file, 2.9 MB.

**FIG S4**, TIF file, 2.6 MB.

**FIG S5**, TIF file, 0.9 MB.

**FIG S6**, TIF file, 0.8 MB.

**TABLE S1**, DOCX file, 0.03 MB.

**TABLE S2**, DOCX file, 0.02 MB.

**TABLE S3**, DOCX file, 0.02 MB.

## ACKNOWLEDGMENTS

We gratefully appreciate financial support of the project by the International Cooperation and Exchange of the National Natural Science Foundation of China (grant no. 31520103918 to Y.-H.L.), the Foundation for Innovative Research Groups of the National Natural Science Foundation of China (grant no. 32121004), the Local Innovative and Research Teams Project of Guangdong Pearl River Talents Program (grant no. 2019BT02N054), and the Innovation Team Project of Guangdong University (grant no. 2019KCXTD001).

J.-F.Z. and L.-X.F. conceived and designed the experiments. Y.-H.L., X.-P.L., J.S., and L.-X.F. supervised the study. J.-F.Z., M.-X.C., M.C., H.Z., F.-T.L., and Q.L. performed the experiments. L.-X.F. and J.-F.Z. analyzed the data and drafted the manuscript. L.-X.F. and J.S. revised the manuscript. All authors approved the final draft.

We declare no competing interests.

## REFERENCES

- Li R, Lu X, Peng K, Liu Z, Li Y, Liu Y, Xiao X, Wang Z. 2020. Deciphering the structural diversity and classification of the mobile tetracycline resistance gene tet(X)-bearing plasmidome among bacteria. *mSystems* 5:e00134-20. <https://doi.org/10.1128/mSystems.00134-20>.

2. Chen C, Cui C-Y, Yu J-J, He Q, Wu X-T, He Y-Z, Cui Z-H, Li C, Jia Q-L, Shen X-G, Sun R-Y, Wang X-R, Wang M-G, Tang T, Zhang Y, Liao X-P, Kreiswirth BN, Zhou S-D, Huang B, Du H, Sun J, Chen L, Liu Y-H. 2020. Genetic diversity and characteristics of high-level tigeicycline resistance Tet(X) in *Acinetobacter* species. *Genome Med* 12:111. <https://doi.org/10.1186/s13073-020-00807-5>.
3. San Millan A, Pena-Miller R, Toll-Riera M, Halbert ZV, McLean AR, Cooper BS, MacLean RC. 2014. Positive selection and compensatory adaptation interact to stabilize non-transmissible plasmids. *Nat Commun* 5:5208. <https://doi.org/10.1038/ncomms6208>.
4. Harrison E, Brockhurst MA. 2012. Plasmid-mediated horizontal gene transfer is a coevolutionary process. *Trends Microbiol* 20:262–267. <https://doi.org/10.1016/j.tim.2012.04.003>.
5. Porse A, Schonning K, Munck C, Sommer MO. 2016. Survival and evolution of a large multidrug resistance plasmid in new clinical bacterial hosts. *Mol Biol Evol* 33:2860–2873. <https://doi.org/10.1093/molbev/msw163>.
6. Biswas S, Li Y, Elbediwi M, Yue M. 2019. Emergence and dissemination of mcr-carrying clinically relevant *Salmonella* Typhimurium monophasic clone ST34. *Microorganisms* 7:298. <https://doi.org/10.3390/microorganisms7090298>.
7. Sun RY, Ke BX, Fang LX, Guo WY, Li XP, Yu Y, Zheng SL, Jiang YW, He DM, Sun J, Ke CW, Liu YH, Liao XP. 2020. Global clonal spread of mcr-3-carrying MDR ST34 *Salmonella enterica* serotype Typhimurium and monophasic 1,4,[5],12:i:– variants from clinical isolates. *J Antimicrob Chemother* 75: 1756–1765. <https://doi.org/10.1093/jac/dkaa115>.
8. García-Fernández A, Carattoli A. 2010. Plasmid double locus sequence typing for IncHII2 plasmids, a subtyping scheme for the characterization of IncHII2 plasmids carrying extended-spectrum beta-lactamase and quinolone resistance genes. *J Antimicrob Chemother* 65:1155–1161. <https://doi.org/10.1093/jac/dkq101>.
9. Fang LX, Jiang Q, Deng GH, He B, Sun RY, Zhang JF, Cen DJ, Miao YY, Wang D, Guo WY, Sun J, Liu YH, Liao XP. 2020. Diverse and flexible transmission of fosA3 associated with heterogeneous multidrug resistance regions in *Salmonella enterica* serovar Typhimurium and Indiana isolates. *Antimicrob Agents Chemother* 64:e02001-19. <https://doi.org/10.1128/AAC.02001-19>.
10. Wu R, Yi LX, Yu LF, Wang J, Liu Y, Chen X, Lv L, Yang J, Liu JH. 2018. Fitness advantage of mcr-1-bearing IncI2 and IncX4 plasmids in vitro. *Front Microbiol* 9:331. <https://doi.org/10.3389/fmicb.2018.00331>.
11. Seaver LC, Imlay JA. 2001. Alkyl hydroperoxide reductase is the primary scavenger of endogenous hydrogen peroxide in *Escherichia coli*. *J Bacteriol* 183:7173–7181. <https://doi.org/10.1128/JB.183.24.7173-7181.2001>.
12. Spanka D-T, Konzer A, Edelmann D, Berghoff BA. 2019. High-throughput proteomics identifies proteins with importance to postantibiotic recovery in depolarized persister cells. *Front Microbiol* 10:378. <https://doi.org/10.3389/fmicb.2019.00378>.
13. Jarvik T, Smillie C, Groisman EA, Ochman H. 2010. Short-term signatures of evolutionary change in the *Salmonella enterica* serovar typhimurium 14028 genome. *J Bacteriol* 192:560–567. <https://doi.org/10.1128/JB.01233-09>.
14. Kosaka H, Oda Y, Uozumi M. 1985. Induction of umuC gene expression by nitrogen dioxide in *Salmonella typhimurium*. *Mutat Res* 142:99–102. [https://doi.org/10.1016/0165-7992\(85\)90047-8](https://doi.org/10.1016/0165-7992(85)90047-8).
15. Bagg A, Kenyon CJ, Walker GC. 1981. Inducibility of a gene product required for UV and chemical mutagenesis in *Escherichia coli*. *Proc Natl Acad Sci U S A* 78:5749–5753. <https://doi.org/10.1073/pnas.78.9.5749>.
16. Oh J-T, Cajal Y, Skowronska EM, Belkin S, Chen J, Van Dyk TK, Sasser M, Jain MK. 2000. Cationic peptide antimicrobials induce selective transcription of micF and osmY in *Escherichia coli*. *Biochim Biophys Acta* 1463: 43–54. [https://doi.org/10.1016/S0005-2736\(99\)00177-7](https://doi.org/10.1016/S0005-2736(99)00177-7).
17. Zheng X, Ji Y, Weng X, Huang X. 2015. RpoS-dependent expression of OsmY in *Salmonella enterica* serovar Typhi: activation under stationary phase and SPI-2-inducing conditions. *Curr Microbiol* 70:877–882. <https://doi.org/10.1007/s00284-015-0802-1>.
18. Yeats C, Bateman A. 2003. The BON domain: a putative membrane-binding domain. *Trends Biochem Sci* 28:352–355. [https://doi.org/10.1016/S0968-0004\(03\)00115-4](https://doi.org/10.1016/S0968-0004(03)00115-4).
19. Weichart D, Lange R, Henneberg N, Hengge-Aronis R. 1993. Identification and characterization of stationary phase inducible genes in *Escherichia coli*. *Mol Microbiol* 10:407–420. <https://doi.org/10.1111/j.1365-2958.1993.tb02672.x>.
20. Bertin Y, Segura A, Jubelin G, Dunieri L, Durand A, Forano E. 2018. Aspartate metabolism is involved in the maintenance of enterohaemorrhagic *Escherichia coli* O157:H7 in bovine intestinal content. *Environ Microbiol* 20:4473–4485. <https://doi.org/10.1111/1462-2920.14380>.
21. Six S, Andrews SC, Unden G, Guest JR. 1994. *Escherichia coli* possesses two homologous anaerobic C4-dicarboxylate membrane transporters (DcuA and DcuB) distinct from the aerobic dicarboxylate transport system (Dct). *J Bacteriol* 176:6470–6478. <https://doi.org/10.1128/jb.176.21.6470-6478.1994>.
22. Suriyanarayanan T, Periasamy S, Lin MH, Ishihama Y, Swarup S. 2016. Flagellin FliC phosphorylation affects type 2 protease secretion and biofilm dispersal in *Pseudomonas aeruginosa* PAO1. *PLoS One* 11:e0164155. <https://doi.org/10.1371/journal.pone.0164155>.
23. Yamazaki S, Takei K, Nonaka G. 2016. ydjN encodes an S-sulfocysteine transporter required by *Escherichia coli* for growth on S-sulfocysteine as a sulfur source. *FEMS Microbiol Lett* 363:fnw185. <https://doi.org/10.1093/femsle/fnw185>.
24. Chonoles Imlay KR, Korshunov S, Imlay JA. 2015. Physiological roles and adverse effects of the two cystine importers of *Escherichia coli*. *J Bacteriol* 197:3629–3644. <https://doi.org/10.1128/JB.00277-15>.
25. Lopez C, Checa SK, Soncini FC. 2018. CpxR/CpxA controls scsABCD transcription to counteract copper and oxidative stress in *Salmonella enterica* serovar Typhimurium. *J Bacteriol* 200:e00126-18. <https://doi.org/10.1128/JB.00126-18>.
26. Hussein SH, Samir R, Aziz RK, Toama MA. 2019. Two putative MmpL homologs contribute to antimicrobial resistance and nephropathy of enterohemorrhagic *E. coli* O157:H7. *Gut Pathog* 11:15. <https://doi.org/10.1186/s13099-019-0296-7>.
27. Cheng X, Wang W, Molineux IJ. 2004. F exclusion of bacteriophage T7 occurs at the cell membrane. *Virology* 326:340–352. <https://doi.org/10.1016/j.virol.2004.06.001>.
28. Domingues CPF, Rebelo JS, Monteiro F, Nogueira T, Dionisio F. 2022. Harmful behaviour through plasmid transfer: a successful evolutionary strategy of bacteria harbouring conjugative plasmids. *Philos Trans R Soc Lond B Biol Sci* 377:20200473. <https://doi.org/10.1098/rstb.2020.0473>.
29. Dorado-Morales P, Garcillán-Barcia MP, Lasa I, Solano C. 2021. Fitness cost evolution of natural plasmids of *Staphylococcus aureus*. *mBio* 12:e03094-20. <https://doi.org/10.1128/mBio.03094-20>.
30. Heuer H, Fox RE, Top EM. 2007. Frequent conjugative transfer accelerates adaptation of a broad-host-range plasmid to an unfavorable *Pseudomonas putida* host. *FEMS Microbiol Ecol* 59:738–748. <https://doi.org/10.1111/j.1574-6941.2006.00223.x>.
31. Gilmour MW, Thomson NR, Sanders M, Parkhill J, Taylor DE. 2004. The complete nucleotide sequence of the resistance plasmid R478: defining the backbone components of incompatibility group H conjugative plasmids through comparative genomics. *Plasmid* 52:182–202. <https://doi.org/10.1016/j.plasmid.2004.06.006>.
32. Consuegra J, Gaffe J, Lenski RE, Hindre T, Barrick JE, Tenaillon O, Schneider D. 2021. Insertion-sequence-mediated mutations both promote and constrain evolvability during a long-term experiment with bacteria. *Nat Commun* 12: 980. <https://doi.org/10.1038/s41467-021-21210-7>.
33. Mahéroul A-C, Kemble H, Magnan M, Gachet B, Roche D, Nagard HL, Tenaillon O, Denamur E, Branger C, Landraud L. 2019. Advantage of the F2:A1:B– IncF pandemic plasmid over IncC plasmids in in vitro acquisition and evolution of blaCTX-M gene-bearing plasmids in *Escherichia coli*. *Antimicrob Agents Chemother* 63:e01130-19. <https://doi.org/10.1128/AAC.01130-19>.
34. Che Y, Yang Y, Xu X, Brinda K, Polz MF, Hanage WP, Zhang T. 2021. Conjugative plasmids interact with insertion sequences to shape the horizontal transfer of antimicrobial resistance genes. *Proc Natl Acad Sci U S A* 118: e2008731118. <https://doi.org/10.1073/pnas.2008731118>.
35. Siguier P, Gourbeyre E, Chandler M. 2014. Bacterial insertion sequences: their genomic impact and diversity. *FEMS Microbiol Rev* 38:865–891. <https://doi.org/10.1111/1574-6976.12067>.
36. Hall JPI, Wright RCT, Harrison E, Muddiman KJ, Wood AJ, Paterson S, Brockhurst MA. 2021. Plasmid fitness costs are caused by specific genetic conflicts enabling resolution by compensatory mutation. *PLoS Biol* 19: e3001225. <https://doi.org/10.1371/journal.pbio.3001225>.
37. Harrison E, Guymer D, Spiers AJ, Paterson S, Brockhurst MA. 2015. Parallel compensatory evolution stabilizes plasmids across the parasitism-mutualism continuum. *Curr Biol* 25:2034–2039. <https://doi.org/10.1016/j.cub.2015.06.024>.
38. Hall JPI, Wright RCT, Guymer D, Harrison E, Brockhurst MA. 2020. Extremely fast amelioration of plasmid fitness costs by multiple functionally diverse pathways. *Microbiology (Reading)* 166:56–62. <https://doi.org/10.1099/mic.0.000862>.
39. Zhang P, Mao D, Gao H, Zheng L, Chen Z, Gao Y, Duan Y, Guo J, Luo Y, Ren H. 2022. Colonization of gut microbiota by plasmid-carrying bacteria is facilitated by evolutionary adaptation to antibiotic treatment. *ISME J* 16:1284–1293. <https://doi.org/10.1038/s41396-021-01171-x>.

40. Billane K, Harrison E, Cameron D, Brockhurst MA. 2022. Why do plasmids manipulate the expression of bacterial phenotypes? *Philos Trans R Soc Lond B Biol Sci* 377:20200461. <https://doi.org/10.1098/rstb.2020.0461>.
41. Brockhurst MA, Harrison E. 2021. Ecological and evolutionary solutions to the plasmid paradox. *Trends Microbiol* 30:534–543. <https://doi.org/10.1016/j.tim.2021.11.001>.
42. Kloos J, Gama JA, Hegstad J, Samuelsen O, Johnsen PJ. 2021. Piggybacking on niche adaptation improves the maintenance of multidrug-resistance plasmids. *Mol Biol Evol* 38:3188–3201. <https://doi.org/10.1093/molbev/msab091>.
43. Li L, Dechesne A, Madsen JS, Nesme J, Sørensen SJ, Smets BF. 2020. Plasmids persist in a microbial community by providing fitness benefit to multiple phylotypes. *ISME J* 14:1170–1181. <https://doi.org/10.1038/s41396-020-0596-4>.
44. CLSI. 2008. Performance standards for antimicrobial disk and dilution susceptibility tests for bacteria isolated from animals; approved standard—3rd ed. CLSI M31-A3. Clinical and Laboratory Standards Institute, Wayne, PA.
45. CLSI. 2019. Performance standards for antimicrobial susceptibility testing. CLSI supplement M100. Clinical and Laboratory Standards Institute, Wayne, PA.
46. Fang LX, Li XP, Li L, Chen MY, Wu CY, Li LL, Liao XP, Liu YH, Sun J. 2018. ISEcp1-mediated transposition of chromosome-borne bla<sub>CMY-2</sub> into an endogenous ColE1-like plasmid in *Escherichia coli*. *Infect Drug Resist* 11:995–1005. <https://doi.org/10.2147/IDR.S159345>.
47. Millan AS. 2018. Evolution of plasmid-mediated antibiotic resistance in the clinical context. *Trends Microbiol* 26:978–985. <https://doi.org/10.1016/j.tim.2018.06.007>.
48. Basan M, Honda T, Christodoulou D, Horl M, Chang YF, Leoncini E, Mukherjee A, Okano H, Taylor BR, Silverman JM, Sanchez C, Williamson JR, Paulsson J, Hwa T, Sauer U. 2020. A universal trade-off between growth and lag in fluctuating environments. *Nature* 584:470–474. <https://doi.org/10.1038/s41586-020-2505-4>.
49. Valle AA-D, León-Sampedro R, Rodríguez-Beltrán J, DelaFuente J, Hernández-García M, Ruiz-Garbajosa P, Cantón R, Peña-Miller R, Millán AS. 2021. Variability of plasmid fitness effects contributes to plasmid persistence in bacterial communities. *Nat Commun* 12:2653. <https://doi.org/10.1038/s41467-021-22849-y>.
50. Sprouffske K, Wagner A. 2016. Growthcurver: an R package for obtaining interpretable metrics from microbial growth curves. *BMC Bioinformatics* 17:172. <https://doi.org/10.1186/s12859-016-1016-7>.
51. Machuca J, Briaies A, Labrador G, Diaz-de-Alba P, Lopez-Rojas R, Docobo-Perez F, Martinez-Martinez L, Rodriguez-Bano J, Pachon ME, Pascual A, Rodriguez-Martinez JM. 2014. Interplay between plasmid-mediated and chromosomal-mediated fluoroquinolone resistance and bacterial fitness in *Escherichia coli*. *J Antimicrob Chemother* 69:3203–3215. <https://doi.org/10.1093/jac/dku308>.
52. Bankevich A, Nurk S, Antipov D, Gurevich AA, Dvorkin M, Kulikov AS, Lesin VM, Nikolenko SI, Pham S, Pribelski AD, Pyshkin AV, Sirotkin AV, Vyahhi N, Tesler G, Alekseyev MA, Pevzner PA. 2012. SPAdes: a new genome assembly algorithm and its applications to single-cell sequencing. *J Comput Biol* 19:455–477. <https://doi.org/10.1089/cmb.2012.0021>.
53. Li R, Yu C, Li Y, Lam TW, Yiu SM, Kristiansen K, Wang J. 2009. SOAP2: an improved ultrafast tool for short read alignment. *Bioinformatics* 25:1966–1967. <https://doi.org/10.1093/bioinformatics/btp336>.
54. Mortazavi A, Williams BA, McCue K, Schaeffer L, Wold B. 2008. Mapping and quantifying mammalian transcriptomes by RNA-Seq. *Nat Methods* 5:621–628. <https://doi.org/10.1038/nmeth.1226>.
55. Alikhan NF, Petty NK, Ben Zakour NL, Beatson SA. 2011. BLAST Ring Image Generator (BRIG): simple prokaryote genome comparisons. *BMC Genomics* 12:402. <https://doi.org/10.1186/1471-2164-12-402>.
56. Wick RR, Judd LM, Gorrie CL, Holt KE. 2017. Unicycler: resolving bacterial genome assemblies from short and long sequencing reads. *PLoS Comput Biol* 13:e1005595. <https://doi.org/10.1371/journal.pcbi.1005595>.
57. Li R, Du P, Zhang P, Li Y, Yang X, Wang Z, Wang J, Bai L. 2021. Comprehensive genomic investigation of coevolution of mcr genes in *Escherichia coli* strains via nanopore sequencing. *Glob Chall* 5:2000014. <https://doi.org/10.1002/gch2.202000014>.
58. Ahmed MN, Porse A, Sommer MOA, Høiby N, Ciofu O. 2018. Evolution of antibiotic resistance in biofilm and planktonic *Pseudomonas aeruginosa* populations exposed to subinhibitory levels of ciprofloxacin. *Antimicrob Agents Chemother* 62:e00320-18. <https://doi.org/10.1128/AAC.00320-18>.
59. Knöppel A, Näsval J, Andersson DI. 2017. Evolution of antibiotic resistance without antibiotic exposure. *Antimicrob Agents Chemother* 61:e01495-17. <https://doi.org/10.1128/AAC.01495-17>.
60. Lu J, Wang Y, Li J, Mao L, Nguyen SH, Duarte T, Coin L, Bond P, Yuan Z, Guo J. 2018. Triclosan at environmentally relevant concentrations promotes horizontal transfer of multidrug resistance genes within and across bacterial genera. *Environ Int* 121:1217–1226. <https://doi.org/10.1016/j.envint.2018.10.040>.
61. Jin M, Lu J, Chen Z, Nguyen SH, Mao L, Li J, Yuan Z, Guo J. 2018. Antidepressant fluoxetine induces multiple antibiotics resistance in *Escherichia coli* via ROS-mediated mutagenesis. *Environ Int* 120:421–430. <https://doi.org/10.1016/j.envint.2018.07.046>.
62. Wang T, Cui Y, Jin J, Guo J, Wang G, Yin X, He Q-Y, Zhang G. 2013. Translating mRNAs strongly correlate to proteins in a multivariate manner and their translation ratios are phenotype specific. *Nucleic Acids Res* 41:4743–4754. <https://doi.org/10.1093/nar/gkt178>.
63. Lian X, Wang X, Liu X, Xia J, Fang L, Sun J, Liao X, Liu Y. 2019. oqxAB-positive IncHI2 plasmid pHX0908 increase *Salmonella enterica* serotype Typhimurium strains tolerance to ciprofloxacin. *Front Cell Infect Microbiol* 9:242. <https://doi.org/10.3389/fcimb.2019.00242>.